

PREPRINT

Author-formatted, not peer-reviewed document posted on 04/03/2025

DOI: <https://doi.org/10.3897/arphapreprints.e151900>

**Temporal Altitudinal Biogeographic Shifts (TABS): R
package for reconstructing biogeographic shifts in
terrestrial and marine habitats over time**

 Johannes De Groeve,  Kenneth Rijdsijk,  Eline Rentier,  Suzette G.A. Flantua, Sietze Norder

1 Research Paper

2

3 **Temporal Altitudinal Biogeographic Shifts (TABS): R package for reconstructing**
4 **biogeographic shifts in terrestrial and marine habitats over time**

5

6 Authors: Johannes De Groeve¹, Kenneth F. Rijdsdijk¹, Eline S. Rentier², Suzette G.A. Flantua²,
7 Sietze J. Norder³

8 1. Institute for Biodiversity and Ecosystem Dynamics, University of Amsterdam,
9 Amsterdam, Netherlands

10 2. Department of Biological Sciences and Bjerknes Centre for Climate Research,
11 University of Bergen, Bergen, Norway

12 3. Copernicus Institute of Sustainable Development, Utrecht University, Utrecht,
13 Netherlands

14 Corresponding author: Johannes De Groeve j.degroeve@uva.nl;
15 degroevejohannes@gmail.com

16 JDG: <https://orcid.org/0000-0002-1274-3237>

17 ESR: <https://orcid.org/0000-0001-6234-1300>

18 SGAF: <https://orcid.org/0000-0001-6526-3037>

19 KFR: <https://orcid.org/0000-0002-0943-2577>

20 SN: <https://orcid.org/0000-0003-4692-4543>

21

22 Abstract

23 Paleoclimatic variations have profoundly influenced the global distribution of ecosystems and
24 habitats, altering their altitude, spatial configuration, area, and connectivity. Notable
25 examples include island archipelagos and alpine biomes, where shifts in sea-levels and forest
26 lines respectively reshaped their spatial structures. To understand how such changes affected
27 species distributions and biodiversity patterns, we require spatially-explicit reconstructions
28 over continuous time series. However, a comprehensive and reproducible methodology that
29 captures their spatio-temporal dynamism is lacking. Here, we introduce the R package
30 Temporal Altitudinal Biogeographic Shifts (TABS), a tool designed for reconstructing spatial
31 configurations over time, focusing on biogeographic systems bounded by an altitudinal range.
32 We demonstrate the use of TABS by modelling spatial configurations ('shapes') of island
33 archipelagos and alpine biomes in response to modulations in sea-levels and forest lines.
34 Unique to TABS, it can also account for crustal deformation due to ice sheet loading and
35 gravitational forces, and for geotectonic and geophysical topographic changes. Beyond past
36 reconstructions, TABS can project spatial configurations shaped by future climatic conditions.
37 This versatile package is easily adaptable to various altitude-bounded biogeographic systems
38 influenced by long-term climatic variations, such as coral reefs and sea shelves. Studying the
39 shifts in biogeographic systems through continuous spatial reconstructions, rather than
40 snapshots in time such as the Last Glacial Maximum, captures the nuances of continuously
41 changing environments and provides a more complete understanding of the biogeography of
42 our planet.

43 Highlights

- 44 ● TABS R package enables detailed spatio-temporal reconstructions of biogeographic
45 systems along altitudinal gradients.
- 46 ● Designed with user-friendliness in mind, it offers a streamlined setup, enabling
47 researchers to start reconstructions quickly without extensive technical expertise.
- 48 ● TABS is applicable to diverse biogeographic systems, including islands, coastal zones,
49 and mountains.
- 50 ● It provides flexibility to tailor input data, parameters, and settings according to
51 specific local conditions and research objectives.
- 52 ● TABS generates outputs using a standardised data structure and open data formats,
53 enabling effective analysis and presentation of results.

54 Keywords

55 Quaternary climate change, sea-level fluctuations, spatio-temporal analysis, habitat
56 modelling, paleogeographical reconstructions, climate-driven ecosystem shifts

57

58

59

60

61

62

63 1 | Introduction

64 Quaternary climate variations have been a significant driver of evolutionary and ecological
65 processes, profoundly influencing the spatial distribution of biogeographic systems, including
66 habitats, ecosystems and their species communities (Hewitt 2000, Rangel et al. 2018).
67 Climatic variations have repeatedly altered coastlines through sea-level changes, leading to
68 changes in the area and connectivity of terrestrial and marine habitats (Fernández-Palacios et
69 al. 2016, Kealy et al. 2017, 2018). These fluctuations have not only transformed land-sea
70 boundaries (Ali and Aitchison 2014, Weigelt et al. 2016, Norder et al. 2019) but also reshaped
71 the distribution of habitats and species across various ecosystems, from coastal zones to
72 mountainous regions (Sandel et al. 2011, Svenning et al. 2015, Flantua et al. 2019). In
73 particular, altitude-driven biogeographic shifts in mountainous areas, where species respond
74 to warming by moving upslope and to cooling by moving downslope, highlight the dynamic
75 relationship between climate and ecosystem distributions (Rull and Nogué 2007, Dirnböck et
76 al. 2011, Flantua et al. 2014, Flantua and Hooghiemstra 2018). Understanding these historical
77 shifts is crucial for anticipating how future climate changes will continue to reshape the
78 biosphere (Williams et al. 2007), including the distribution of human populations (Wetzel et
79 al. 2012).

80

81 Spatio-temporal reconstructions of biogeographic systems are essential for understanding
82 the complex responses of ecosystems to Quaternary climate fluctuations. By quantifying past
83 habitat extent, configuration, and connectivity, these reconstructions provide critical insights
84 into past species distributions. For instance, they allow the identification of key areas, such as
85 refugia and migration routes (Comes and Kadereit 1998) and to find evidence for hypotheses

86 on dispersal among islands in archipelagos (Ali and Aitchison 2014, Rijdsdijk et al. 2014a).
87 Especially spatio-temporal reconstructions that analyse changes across longer, continuous
88 time scales provide a more nuanced understanding of biogeographic dynamics than analyses
89 focused on a snapshot in time (Flantua et al. 2019, 2020, Norder et al. 2019). By examining
90 how habitats shifted their distributions across various temporal intervals, we can reveal
91 complex biogeographic patterns of expansion and contraction, and isolation and connectivity,
92 that are otherwise not evident when focusing on isolated time points. Such long-term
93 reconstructions can assess the cumulative effects of climatic fluctuations on islands, such as
94 the effect of changing gene flow (Papadopoulou and Knowles 2015, 2017) and island
95 endemism over time (Ali and Aitchison 2014, Rijdsdijk et al. 2014b, Fernández-Palacios et al.
96 2016). In addition, spatio-temporal connectivity can be quantified to test how changes in
97 habitat (size and suitability) and configuration changed over time (Martensen et al. 2017,
98 Flantua et al. 2019, Huang et al. 2020). This broader temporal perspective of the dynamics of
99 terrestrial and marine habitats worldwide is essential to enable a deeper understanding of
100 how past environments influenced present-day biodiversity, and to provide better predictions
101 of the effect of habitat isolation and connectivity in response to future climate change
102 (McGuire et al. 2016).

103

104 Despite the broad interest in spatio-temporal reconstructions, important limitations remain.
105 A key limitation is the absence of a widely accepted, standardised workflow for reconstructing
106 spatio-temporal biogeographic shifts across different systems. Workflows that can seamlessly
107 integrate data from paleoclimatology, geology, ecology, and biogeography are currently
108 absent. Especially the integration of tectonic and isostatic processes is of vital importance for

109 accurate reconstructions in island systems (Whittaker et al. 2017). In addition, numerous
110 studies often rely on discrete temporal snapshots, which fail to capture continuous transitions
111 and cumulative effects critical to understanding long-term biogeographic patterns (Flantua et
112 al. 2020). Also, many workflows may not be easily adaptable across different systems, scales,
113 or temporal resolutions, restricting their application for interdisciplinary adaptability and a
114 broader research community, along with extensive data preparation and technical expertise.
115 Moreover, there is a lack of tools that simultaneously reconstruct past shifts and project
116 future changes under various climate scenarios. Finally, current workflows often fail to
117 provide outputs in open, compatible formats that facilitate further analysis and
118 interdisciplinary collaboration. To address these gaps and advance our understanding of
119 biogeographic dynamics across both space and time, the development of a versatile, user-
120 friendly workflow is essential.

121

122 Here, we introduce a globally applicable, reproducible workflow for reconstructing
123 biogeographic shifts in terrestrial and marine environments in response to climate,
124 topography, and geological changes. The Temporal Altitudinal Biogeographic Shifts (TABS) R
125 package models spatial configurations over time, focusing on biogeographic systems bounded
126 by an altitudinal range. Additionally, TABS integrates corrections for crustal deformations and
127 gravitational forces using advanced geophysical models, as opposed to earlier models that
128 often neglected geological dynamics and local context (Rijsdijk et al. 2014b, Norder et al.
129 2018, Tan et al. 2023). It also allows for adjustments based on local geological conditions,
130 including uplift and subsidence. Furthermore, we expanded its application to mountain
131 systems, building on previous work (Flantua et al. 2019, 2020). TABS is highly versatile,

132 enabling easy modification of input data and parameters to suit local conditions. It produces
133 rapid, accurate reconstructions with minimal manual input, facilitating the modelling and
134 quantification of habitat changes across time. TABS generates outputs that are analytically
135 robust and well-suited for further analysis and publication.

136

137 [2 | Methods: TABS workflow](#)

138 [2.1 | Functionality](#)

139 The functionality of TABS (Temporal Altitudinal Biogeographic Shifts) builds on and automates
140 the foundational work laid out by Norder et al. (2018), who developed an R-based workflow
141 to produce a global island and archipelago configuration database. The study combined a
142 global eustatic sea-level curve with a topographic-bathymetric model to reconstruct island
143 area change and configurations, including labelling of individual present and past island
144 polygons. While the workflow from Norder et al. (2018) required manual re-runs to
145 incorporate new datasets, TABS introduces a dynamic, customisable framework. It allows
146 iterative reconstructions that can be fine-tuned based on varying climate and geological
147 conditions and flexible automated label definitions, representing a major leap forward in
148 modelling environmental dynamics. TABS further builds on early work, including the detailed
149 spatio-temporal reconstruction model developed by Simaiakis et al. (2017) further improved
150 by (Rijsdijk et al. 2025) for the Ionian and Aegean sea extents. Both models track island
151 dynamics over the past 26,000 years, but different from Norder et al. (2018) these studies
152 account for local variations in sea-level changes. The latter study also accounts for geological
153 changes to account for the region's tectonic activity. The integration of such complex
154 reconstruction efforts in TABS demonstrated the capacity to model highly complex

155 biogeographic systems with high temporal and spatial resolution. TABS has further expanded
156 to encompass other biogeographic systems, such as high altitude mountain ecosystems,
157 where altitudinal shifts due to temperature changes during the Quaternary period mirror sea-
158 level driven island dynamics (Flantua et al. 2019, 2020). The R package also supports
159 applications for marine biogeographic systems, like the reconstruction of coral reef and shelf
160 sea distributions since the Last Glacial Maximum (De Groeve et al. 2022a). Using a
161 comprehensive set of global datasets and parameter settings, TABS enables the creation of
162 spatial-explicit models representing biogeographic systems worldwide. The next paragraphs
163 describe main datasets and function parameters used by the core function of TABS:
164 *reconstruct*.

165

166 2.2 | Global Datasets

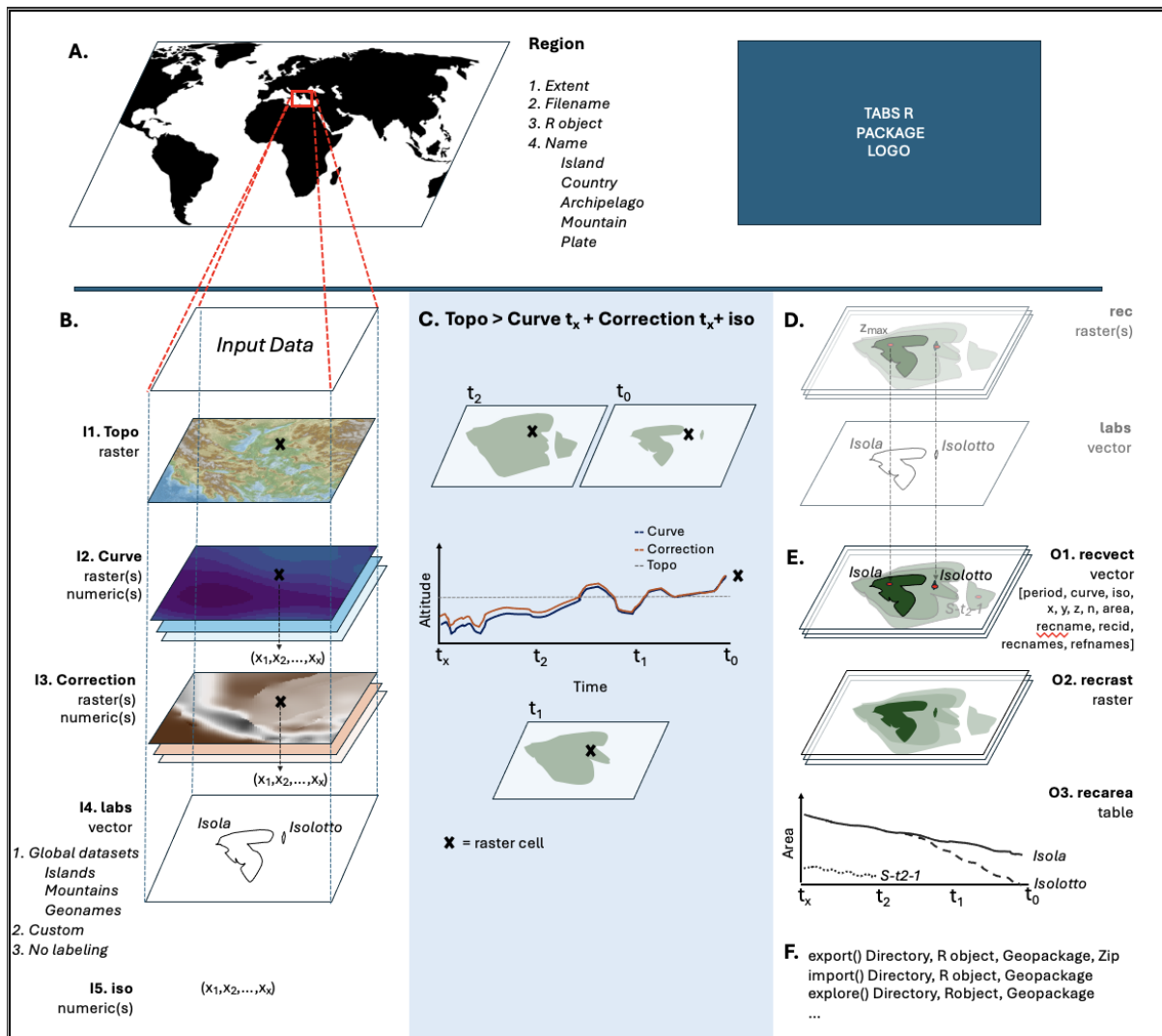
167 TABS allows for generating reconstructions using region-specific custom data sources, but
168 various built-in datasets can be used to create reconstructions anywhere on the globe. To
169 enable these datasets, first-time users are encouraged to run the *setup* function, which
170 creates a directory structure in a specified or default local path, and automatically downloads
171 these datasets (requiring 15 GB of disk space). Datasets include: i) a tiled version of the global
172 bathymetry and topography (GEBCO Bathymetric Compilation 2024), ii) a spatio-temporal
173 sea-level curve, iii) labelling datasets, including the Global Shoreline Vector (GSV, Sayre et al.
174 2019), bioclimatic and physical characterisation of the worlds' islands (Weigelt et al. 2013a,
175 2013b), tectonic plates and orogens (Bird 2003), an open source labelling points dataset for
176 many types of features (GeoNames 2023) and the Global Mountain Biodiversity Assessment
177 (GMBA) Mountain Inventory v2 (Snethlage et al. 2022). These datasets are made available via

178 Figshare to facilitate and manage any future changes (De Groeve et al. 2022b, 2023, 2024).
179 For instance, the GEBCO model is updated on an annual basis and we aim to upload and
180 announce the integration of most recent versions with upcoming TABS version releases. For
181 more details on dataset sources and examples see vignettes at the TABS website.

182

183 2.3 | *Reconstruct* function

184 The *reconstruct* function is the core function of the TABS R-package and operates with
185 several integrated helper or utility functions (Fig. 1). The purpose of this function is to
186 reconstruct and label past or future changes in terrestrial or marine biogeographic systems
187 for a specific region in response to changes in climate and geology. These reconstructions are
188 generated by intersecting a bathymetric or topographic model with a (spatio-temporal) curve
189 and optionally correcting it for regional topographic changes. The resulting reconstructed
190 spatial configurations (hereafter “shapes”) of the biogeographic system of interest are
191 optionally named using a labelling dataset. The *reconstruct* function has six main input
192 parameters (*region*, *reclabs*, *topo*, *curve*, *iso*, *correction*) and several
193 additional parameters (*buffer*, *noise(rm)*, *aggregate*, *fact*, *units*,
194 *fillholes*, *metrics*) that can further fine-tune reconstructions in accordance with the
195 users’ needs.



196

197 **Fig. 1. The infographic provides a summary of the TABS R package and the steps**
 198 **incapsulated by the function *reconstruct*.** (A) A region of interest on the globe can be selected
 199 using a wide range of methods, including by extent, filename, R objects (e.g., *qs2*), or
 200 geographic names such as islands, countries, archipelagos, mountains, and tectonic plates.
 201 (B) For the selected region, a harmonized input data brick is prepared, which includes
 202 topography (*topo*, I1), *curve* (I2), *correction* (I3), labels (*labs*, I4), and the altitudinal offset (*iso*,
 203 I5). Each dataset can be customized, and both *curve* and *correction* support various formats,
 204 including numeric vectors or raster(s). The latter two datasets are intersected with the region
 205 of interest and resampled to the resolution of the topography. If needed, the *correction*
 206 dataset is also aligned to the temporal resolution of the curve. The *labs* dataset can be one of
 207 the default global datasets (e.g., islands, mountains, geonames), a custom column name, or
 208 labelling can be ignored altogether. The *iso* variable defines the altitudinal offset from the
 209 curve for a biogeographic system (e.g., corals between 0–30 m BSL), and in this example, it is
 210 set to 0. (C) Reconstructed shapes are calculated as topographic pixels higher than the sum
 211 of the *curve* and *correction*. A line graph illustrates the interaction between these three
 212 variables (*topo*, *curve*, *correction*) for a single pixel (cross-marked), showing reconstructed
 213 shapes for three timestamps (t_0 , t_1 , t_2). At t_0 , the pixel remains below the combined curve-
 214 correction threshold, but exceeds it at t_1 and t_2 , resulting in reconstructed shapes. (D/E) The

215 generated shapes are then labelled by identifying the highest point in the reconstructed
216 shapes and intersecting them with the labelling dataset. Emerging shapes (e.g., at timestamp
217 t_2) are named using a standard convention (e.g., 'S' for shape, time of disappearance, and an
218 identifier). Each shape is also assigned spatial attributes, such as the period, curve and iso,
219 the area (in m^2 and raster cells), x, y, z coordinates, a list of intersecting present-day labels
220 from the labs dataset, and a record of all reconstructed shapes intersecting with the shape at
221 timestamp t_x . **(E)** The *reconstruct* function results in three output datasets: reconstructed
222 shapes in vector and raster formats (*recvect*, *recrast*), and reconstructed area estimates for
223 each shape (*recarea*). **(F)** The final dataset collection includes all the necessary datasets to
224 reproduce the workflow, including all in-and outputs. The dataset collection can be exported,
225 imported, and explored visually using various open data formats, including a (zipped)
226 directory, R object, and geopackage.

227

228 **Region** parameter:

229 To generate a TABS reconstruction, it is important to first define and select the region of
230 interest, which can be done using one of five approaches (**Table 1**): (i) interactive drawing of
231 an extent, (ii) extent coordinates, (iii) path to a local spatial dataset, (iiii) a *sf* or *spatVector* R-
232 object, and (iiiiii) region-name definitions including islands, archipelagos, countries, tectonic
233 plates and mountains. In total 32,255 region name-definitions are implemented in TABS that
234 can be explored using the built-in *regions* dataset. See more details on region selection on the
235 TABS website's vignettes.

236

237 **Table 1. Values and descriptions for the *Region* argument**

Description	Value
Default; Interactive drawing of an extent or polygon within R session	region=NULL
Specifying the extent as vector or ext-object	region=c(xmin,xmax,ymin,ymax)
A path to a locally stored spatial dataset (e.g. shapefile, geopackage)	region='filename'
A spatial (sf, SpatVector) object containing points or shapes	region='spatvector'
A name of an island, archipelago, country, tectonic plate or mountain	region='Greece' region='Sporades'

238

239 ***reclabs*** parameter:

240 TABS facilitates labelling of the biogeographic shapes, i.e. naming of each reconstructed
 241 shape. To assign such labels, the user can specify the *reclabs* parameter, which includes
 242 three approaches ([table 2](#)). Specifically, (i) labelling using the islands, mountains or geonames
 243 global datasets (see 2.2. global datasets), (ii) custom labelling and (iii) automated labelling.
 244 With the parameter *aggregate* (boolean; TRUE/FALSE) the spatial scale at which to perform
 245 labelling can be defined, specifically for the whole region or for individual reconstructed
 246 shapes. For more information on the automatic assigning of labels, see the TABS website's
 247 vignettes.

248

249 **Table 2. Values and descriptions for *Reclabs* argument**

Description	Value
labelling using the islands, mountains or geonames global datasets	reclabs='isls' reclabs='mnts' reclabs='peak'
Custom labelling by specifying the column name of a user-defined region-object	reclabs='name'
Automatically generated labels	reclabs=FALSE
Default; No labelling dataset defined; Labelling depends on the input of the region-object	reclabs=NULL

250

251 ***Topo*** parameter:

252 By default, the GEBCO grid (2024) is used as the topographic (*topo*) object and consists of
 253 both bathymetry and topography at a global scale at a resolution of 30 arcseconds.
 254 Alternatively, the user can specify a regional digital elevation model as a path (e.g.,
 255 `topo='path_to_file.tif'`). TABS automatically extracts the highest point identified in
 256 the topographic object, which is used for labelling reconstructed shapes. The spatial
 257 resolution of the *topo* object will be assigned to the TABS outputs (as produced by the
 258 *reconstruct* function), unless the resolution factor (*fact*) is modified. Outputs are assigned
 259 the projection system of the input *topo* object.

260

261 ***Curve*** parameter:

262 The spatio-temporal curve can be defined as any dataset which expresses the relative shift in
 263 altitude over time for the biogeographic system of interest. Curves can vary both in space and
 264 in time within a region, thus it can be a vector of one or more altitude values, or one or more
 265 rasters. A typical example of a curve is a sea-level curve, expressing the change in sea-level

266 compared to the present-day reference (i.e. 0 m RSL). Another example is the upper forest
267 line (UFL), expressing the maximum altitude above present day sea-level at which continuous
268 forest habitat persists. A curve can also be defined by a single value, for instance, the median
269 sea-level across the Pleistocene or a future scenario of sea-level rise. Hence, TABS allows a
270 flexible and customisable definition of a curve. TABS has several built-in curves that can be
271 called by their name (**Table 3**). These curves represent different global sea-level curves (past
272 and future), and an example of a UFL curve for the Northern Andes (*funza*; Torres et al. 2005,
273 Flantua et al. 2019). Note that the shift in altitude should use the same unit as the *topo*
274 object, which is usually expressed in meters. For more details, see the TABS website's
275 vignettes.

276

277 **Table 3. Spatial-temporal curves**

Name	Description	Time span	Temporal resolution (time steps)	Spatial resolution	Source
Lambeck curve='Lambeck'	Global eustatic sea-level curve	35 kyr BP	1000 yr	NA	Lambeck et al. 2014
Cutler curve='Cutler'	Global eustatic sea-level curve	120 kyr BP	1000 yr	NA	Cutler et al. 2003
Bintanja curve='Bintanja'	Global eustatic sea-level curve	3 Myr BP	1000 yr	NA	(Bintanja and van de Wal 2008)
De Groeve curve='st_curve'	Global spatio-temporal sea-level curve	26 kyr BP	500 yr	0.2°	(De Groeve et al. 2022a)
IPCC curve='SSP1'	The global average sea-level for four IPCC scenarios (SSP1, SSP2, SSP3, SSP5).	Present day to 2100	20 yr (near, medium, long term)	NA	Intergovernmental Panel on Climate Change (IPCC) 2023
Funza curve='Funza'	Upper forest line altitudes derived from fossil pollen record Funza (Colombia)	1 Myr BP – 22 kyr BP	29-1000 kyr	NA	Torres et al. 2005, Flantua et al. 2019
User-defined	A vector with the altitude(s) or a data frame containing altitudes at different time steps.	Any	Any	Any	NA
NULL	If no argument is provided, construction will be produced for the present				

278

279

280 ***Iso*** parameter:

281 The *iso*(hypse) argument defines the offset from the curve and covers the altitudinal range
282 of the biogeographic system to reconstruct. By default, this argument is set to 0 meter to
283 reconstruct configurations of coastlines and forest lines, but any altitudinal range that
284 describes the altitudinal distribution of a biogeographic region can be used. For example, the
285 availability of corals and shelf seas vary synchronously with sea-level change, thus to
286 reconstruct their spatial configurations we need to specify the minimum and maximum
287 altitude range at which they may occur, respectively 0-30 m BSL and 0-140 m BSL.

288

289 ***Correction*** parameter:

290 The reconstruction of biogeographic systems and their spatial configurations over time is
291 influenced not only by specific climatic conditions but also by geotectonic and geophysical
292 activities that result in topographic changes during the study period. For instance, whether
293 an island is above or below the sea-level will not only depend on the redistribution of water
294 from ice sheets, but also local effects that change the topography: such as uplift and
295 subsidence in tectonic active areas, deposition and erosion of sediment in fluvial deltas and
296 land-loss due to catastrophes such as volcanic eruptions. To account for these types of local
297 topographic changes, a *correction* parameter can be defined accounting for (1) temporal
298 linear topographic changes expressed as a rate over time (e.g. mm/yr) and (2) temporal
299 varying topographic changes. Temporal linear topographic changes are expressed in TABS as
300 a single value or raster. Temporally varying topographic changes are expressed as a vector of
301 values, or a list of rasters. Although a database with global correction rates or values does not
302 yet exist, user-defined corrections can be provided for specific regions. As an example, TABS

303 has one built-in regional correction dataset for uplift and subsidence rates in the Sporades,
304 Greece (Rijsdijk et al. 2025). For more details, see the TABS website's vignettes.

305

306 ***Other parameters***

307 In addition to these six main input parameters of *reconstruct*, there are other settings that
308 can be tailored to specific purposes ([Table 1](#)). A *buffer* can be defined to increase the extent
309 of the *region* definition. With *fillholes*, remaining holes in reconstructed shapes are
310 removed. Further it is possible to identify and remove reconstructed shapes below a specific
311 size (with the *noise* and *noiserm* parameters respectively) and to generate outputs at lower
312 spatial resolution (*fact*). Both *noise(rm)* and *fact* will reduce computation time, since
313 the former will decrease the number of spatial features, and the latter reduces the number
314 of output cells in rasters. The *metrics* parameter specifies which metrics are by default
315 computed, currently only including the area change over time. Moreover, several steps of the
316 *reconstruct* function can be run separately using specific helper-functions, including
317 *get_region*, *get_curve* and *get_correction*.

318

319 [2.4 | TABS outputs](#)

320 The two main outputs of the *reconstruct* function are 1) the reconstructed biogeographic
321 shapes at each time step in raster (*recrast*) and vector (*recvect*) format, and 2) a table with
322 the area for each reconstructed shape (*recarea*) per time step and a unique ID assigned to
323 each shape. These IDs allow for tracking which present-day shapes were merged into larger
324 shapes at different time steps. In addition, all preprocessed input datasets are also provided

325 for the defined region (i.e., *topo*, *labs*, *curve*, *correction*). The reconstruct output can be
326 exported in four file formats: (1) directory, where rasters are exported as GEOTIFF and vectors
327 in GeoPackage, (2) zip, a zipped version of directory-type export, (3) rds/qs2, as the default R
328 export data format and (4) gpkg, a full integration of all outputs in a GeoPackage. Outputs can
329 be exported by specifying the argument *filename*, including the path and optional extension
330 in the *reconstruct* function or in the *export* function. Also an *import* function is
331 available which allows to load the directory, rds/qs2 or GeoPackage as an R object of class
332 *tabs*.

333

334 In addition to these in- and outputs that are stored locally, an R object of class *tabs* will be
335 generated that can be used to explore the outputs interactively with the *explore* function.
336 This function will generate interactive maps to visually explore biogeographic shapes over
337 time, or to compare reconstructed shapes to their present-day distribution.

338

339 [3. Results: examples of use cases](#)

340 [3.1 | Case study 1: Coastlines - Sporades \(Greece\)](#)

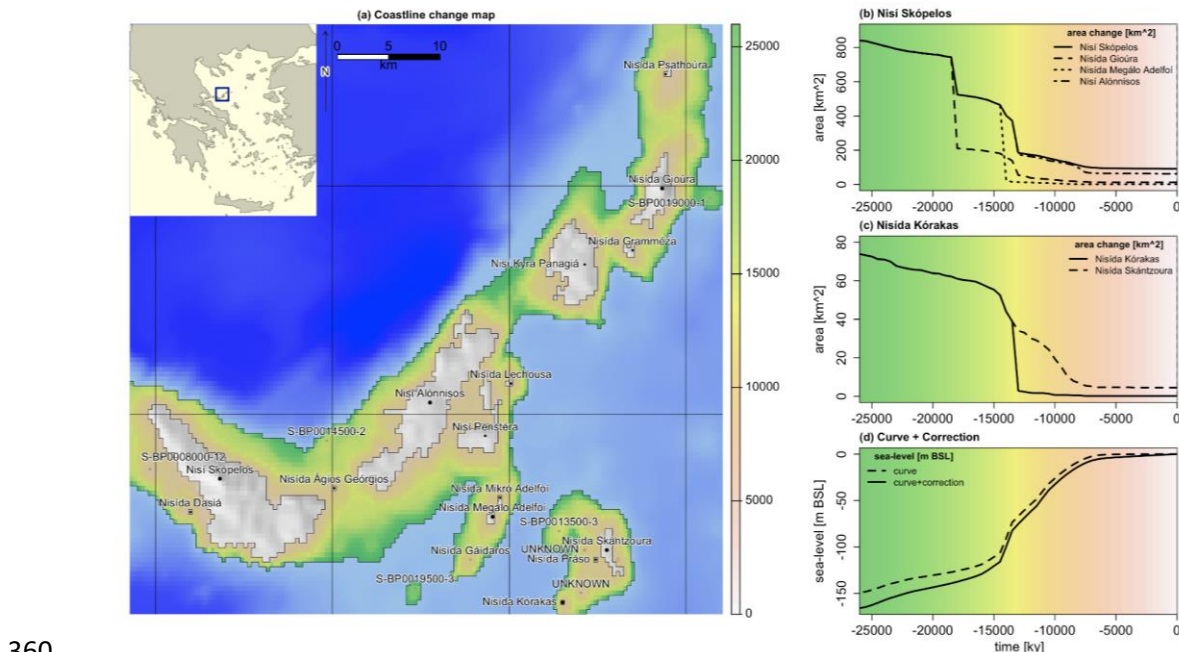
341 As a first case study, we reconstructed the coastlines of the Sporades in Greece since the LGM
342 (26 kyr BP) to the present-day using the default input datasets (*topo*, *labs*, *curve*). In addition,
343 we defined a correction grid to account for local changes in uplift and subsidence (sample
344 dataset in TABS). Such a complex reconstruction can be run simply by defining four
345 parameters: (1) *region*, as the extent of the correction, (2) *reclabs*, to specify the labeling
346 dataset, (3) *correction*, to account for topographic changes over the last 26 kyr BP and (4)

347 *curve*, set to the spatio-temporal sea-level curve by De Groeve et al. (2022; [Table 2](#)). Note
 348 that inputs *topo* and *labs* are also available as built-in datasets for the extent of the Sporades,
 349 but if the default datasets have been downloaded using *setup* it is not necessary to specify
 350 the arguments.

351

```

352 # load built-in correction grid
353 correction <- sporades()$correction
354
355 # reconstruct
356 sporades <- reconstruct(region=ext(correction),
357                          reclabs="isls", # island labeling dataset
358                          correction = correction,
359                          curve='st_curve') # call De Groeve curve
    
```



360

361 **Fig. 2. TABS Reconstruction using the built-in dataset of the Sporades islands (Greece).** (a)
 362 Coastline change map. Nisi Skópelos (b) and Nisida Kórakas (c) as “macro-islands” tracked

363 through time. Lines indicate the island areas (y-axis, km²) at different moments in time (x-
364 axis, yr BP). Separating lines indicate different islands as connections are lost due to changing
365 sea-levels. (d) Sea-level fluctuations at different moments in time (x-axis, yr BP) with and
366 without topographic corrections.

367

368 Using the *reconstruct* outputs of TABS, we can create, for example, coastline change maps
369 or graphs representing area change and island connectivity since the LGM due to sea-level
370 fluctuations (Fig. 2). Two island groups remained disconnected from each other (Fig. 2a), here
371 labelled after the highest island of each group, namely Skopelos (Fig. 2b) and Korakas (Fig.
372 2c). Graphs show that most islands within the Sporades archipelago were connected between
373 25-18 kyr BP. More specifically, 13 of the 18 present-day islands were interconnected 24 kyr
374 ago, forming the Skopelos island group, while the other 5 present-day islands formed the
375 Korakas island group 14 kyr ago. In addition, five paleo-islands (non-existing islands in
376 present) emerged within the Sporades, of which three merged with the Skopelos island group
377 (S-BP0014500-2, S-BP0008000-12, S-BP0019000-1), one with the Korakas island group (S-
378 BP0013500-3) and one emerged as a separate island 19.5 kyr ago (S-BP0019500-3).

379

380 3.2 | Case study 2: Mountains – Andes, Venezuela

381 In our second case study, we reconstruct the area change of the ‘páramos’ UFL, i.e. high
382 altitude mountain ecosystem in Venezuela (Northern Andes), during the last 1 million years
383 following Flantua et al. (2019). The authors used the reconstructed altitudes of the UFL, based
384 on the long fossil pollen record Funza (Torres et al. 2005), to delimit the lower boundary of
385 the páramos through time. For the implementation of TABS, we used *reconstruct* without
386 labelling and correction grid, while using the default *topo*. Instead of using the entire curve,
387 we calculated decile statistics, representing the proportion of time that the Funza UFL is

388 higher than the given threshold using proportion steps of 0.1. For example, for a proportion
 389 of 0.1, the altitude will be above a given UFL-value for 10% of the time (approx. 100 kyr). For
 390 these 10 decile-curve values, we ran the *reconstruct* function that provided the data
 391 outputs necessary to generate the decile map, the curve, and area change in relation to the
 392 forest line deciles (Fig. 3 a,b,c). In addition, we also ran the *reconstruct* function from 130-
 393 29 kyr BP to map the area change over the latter period (Fig. 3 d).

394

```

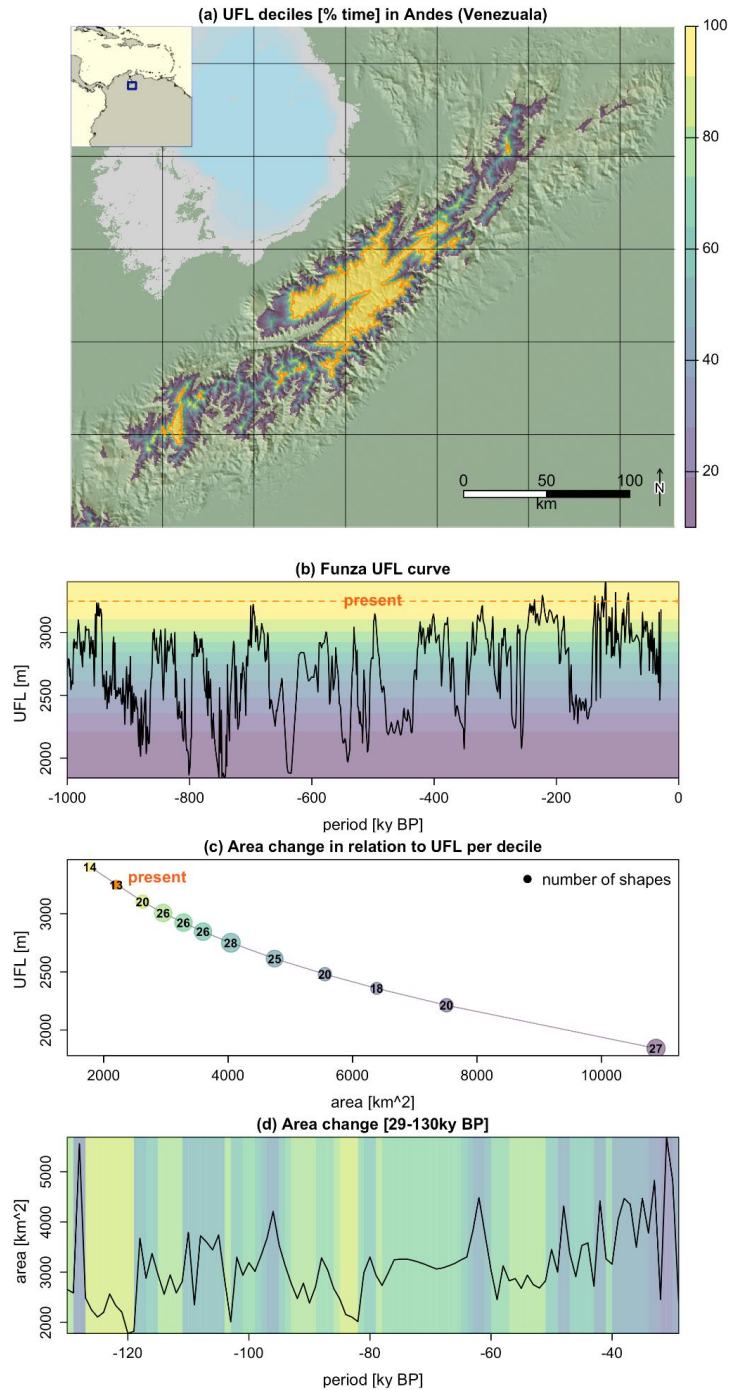
395 # define region using extent coordinates
396 region <- terra::ext(c(-72.5,-69.2,7.5,10.2))

397 # curve
398 curve <- funza[2:length(funza)]

399 # calculate forest line deciles from curve
400 deciles <- quantile(curve, probs = seq(0, 1, by = 0.1))
401
402 # reconstruct forest line deciles
403 andes <- reconstruct(region=region,
404                     curve=deciles,
405                     reclabs=FALSE,
406                     aggregate=TRUE)

407 # reconstruct 0-130 kyr BP
408 andes130 <- reconstruct(region=region,
409                        curve=funza[1:(130-27)],
  
```

410 reclabs=FALSE,
 411 aggregate=TRUE)
 412



413

414 **Fig. 3. Reconstructing upper forest line (UFL) deciles, representing the proportion of time**
 415 **during the last 1 million years that the UFL was above an altitudinal threshold. (a) The map**

416 represents the proportion of time (1000-29 kyr BP) that a pixel was above the UFL threshold.
417 (b) Graph shows the altitudinal variation of the Funza UFL from 1000-19 kyr ago with the
418 colored deciles on the background showing the UFL altitudinal range of each decile. (c) Area
419 change in relation to UFL deciles, where the dots show the number of individual “páramo sky
420 islands” at each decile. (d) Area change curve for the last 29-130 kyr BP.

421 We can see that the present upper forest line (here standardized to UFL = 3250 mASL) is
422 within the upper decile (UFL > 3105 mASL; 2627 km²), resulting in one of the smallest areal
423 extensions (i.e. 2203 km²) of the Páramo in comparison to the last 1 million years. More
424 precisely, only for about 13 kyr, or 1.3 % of the time, the UFL was higher and the
425 corresponding area smaller than the present. Half of the time (500 kyr; middle decile) the UFL
426 was below 2750 mASL resulting in the Páramo to be 1.84 times (> 4044 km²) larger than the
427 present. For 10% of the time (100 kyr; lower decile), the UFL was as low as 2213 mASL,
428 resulting in an areal extension that is about 3.4 times (>7510 km²) larger than the present
429 (2230 km² for a UFL of 3250 mASL).

430

431 [Discussion and future directions](#)

432 Here we present TABS as a workhorse for modelling and quantifying spatio-temporal
433 dynamics of biogeographic systems in response to climate and geology. It is built in such a
434 way that it can be used for any biogeographic system that can be roughly defined by an
435 altitudinal range. Specifically, we modelled shorelines of the Sporades archipelago (Greece)
436 and the upper forest lines delimiting the lower boundary of the ‘Páramos’ (high altitude
437 mountain ecosystem of the Northern Andes) as case studies to showcase TABS’ functionality.
438 These case studies illustrate that TABS requires very limited lines of code and a limited
439 number of parameter settings to reconstruct biogeographic shapes over time. While it is easy
440 to generate such reconstructions using default settings, we showcased that TABS is also highly

441 flexible and can incorporate diverse curve representations including RSL rasters in the first
442 use case and (aggregated) UFL vectors in the second. Thanks to TABS' interoperable and
443 standardised output structure, results can be turned into insightful visualisations to
444 investigate patterns of changing biogeographic systems over time. For example, the first use
445 case illustrates the ease of performing automated labelling procedures for both present-day
446 and submerged islands, and how these outputs can be transformed into maps and graphs to
447 analyze past dynamics of island connections. The second use case illustrates how curve (UFL)
448 statistics (i.e. deciles) formalizing boundaries of a biogeographic system can be turned into
449 insightful maps and graphs, representing surface area trends of a system experiencing
450 contraction over time. In short, we illustrated TABS potential to facilitate and enrich scientific
451 analyses with strong visualisations supporting a broad range of biogeographic studies.

452

453 Some existing software tools, especially used in the field of island biogeography, are
454 complementary to TABS. The *PLeistoDist* R-package (Tan et al. 2023) focuses on visualising
455 and quantifying the effects of eustatic sea-level changes on islands throughout the
456 Pleistocene, providing tools for generating maps and calculating geomorphological metrics.
457 To reconstruct past island areas, *PLeistodist* relies on a global eustatic sea-level curve but
458 does not account for other types of topographic changes due to geological and
459 geomorphological processes (Tan et al., 2023). In contrast, TABS has a suite of built-in curves,
460 including a spatio-temporal curve that accounts for local sea-level variations (De Groeve et al.
461 2022a). Furthermore, new and improved spatio-temporal sea-level models, or other curves
462 (e.g. UFL curves), can be easily integrated in TABS. The R-package *DAISIE* (Valente et al.
463 2015) models island biota change dynamically through speciation, immigration, and

464 extinction, using phylogenetic trees to estimate colonisation, speciation, and extinction rates.
465 In the future, we aim to link or integrate TABS with complementary tools like *PleistoDist*
466 and *DAISIE*, enabling the use of TABS outputs to improve predictions of colonization,
467 speciation, and extinction rates, as well as calculations of geomorphological metrics.

468

469 The performance of TABS is dependent on the complexity of the reconstruction. For instance,
470 generating reconstructions using GEBCO and an eustatic curve, which has been the practice
471 in literature until now (Norder et al. 2018, Tan et al. 2023), will be significantly faster than a
472 reconstruction using high-resolution, local topographic models and spatio-temporal curves.
473 Accounting for local variations by defining a correction grid will further decrease the speed of
474 calculations but will result in more accurate reconstructions. Hence there is a tradeoff
475 between performance and accuracy of the reconstruction and its derived metrics such as area
476 change. The resolution of the input topographic dataset will largely define the quality of the
477 labelling and recognition of shapes. The higher the resolution of the *topo* dataset, the
478 more likely that labelling is done correctly, and the more likely that shapes are identified as
479 separate units. For instance, islands separated by narrow sea streets, like Sicily from mainland
480 Italy and Evia from mainland Greece, will not be distinguished as separate shapes and be
481 included in the continent if no accurate topographic model is available. Also, small shapes,
482 such as islets, will be much better identified using accurate topographic models.

483

484 Improvements and future developments TABS

485 **Global vs regional reconstructions:** Currently, TABS is customised for regional reconstructions
486 across the globe and not for continuous global reconstructions, such as the global shoreline

487 and shelf sea rasters (De Groeve et al. 2022a). Such global reconstructions are also aimed to
488 be integrated in a future release of TABS. However, TABS can be used for global studies by
489 subsequent definition of extents, for instance a list of archipelagos. Using standard iteration
490 functions (*e.g. sapply, lapply*), biogeographic systems can then be reconstructed for each
491 subsequent area of interest.

492

493 **Naming:** Automated labelling of biogeographic shapes is currently only integrated for
494 shoreline objects (continents, islands, islets) and mountain ranges. The default labelling
495 option is based on GSV (Sayre et al. 2019) for shoreline shapes, or GMBA (Snethlage et al.
496 2022) for mountain shapes. Hence, labelling based on other geotags, such as coral bed names,
497 requires the definition of custom labelled points or shapes. When using custom points, it is
498 essential to define locations that have a high probability to fall within the present-day
499 biogeographic shapes (such as highest points or centroids), otherwise, points might not
500 intersect with the reconstructed shapes. Another approach could be to export first a present-
501 day reconstruction, to explore which reconstructed shapes are recognised, edit the shape
502 names, and use this input as the labelling dataset.

503

504 Furthermore, labelling of reconstructed shapes is primarily based on the location of the
505 highest point observed within the underlying topography. This is a valid naming convention
506 for biogeographic systems which only have a lower range limit, such as shorelines as well as
507 upper forest lines, but not for biogeographic systems defined by a range, such as corals or
508 shelf seas. This is because the highest point is not constant and shifts horizontally with every
509 sea-level change. A more advanced procedure is required to enable labelling of shapes during

510 horizontal biogeographic shifts. Reconstructions that do not require labelling or only require
511 area change reconstructions at the extent level are applicable for any biogeographic range
512 definition.

513

514 **Corrections:** While corrections can be integrated in the model, either through definition of a
515 (list of) grids or values, it is expected from the user to prepare this input. This is particularly
516 time consuming if corrections are defined as grids requiring potential data collection,
517 integration and manipulation. Given that there are no integrated databases including rates of
518 topographic change (e.g. uplift, subsidence, erosion, sedimentation) a user will need to first
519 screen the literature to collect known rates for locations within the study area. These rates
520 can be digitised as linear features, in case of linear breakpoints, or as point features, in case
521 rates are known for a specific location. Further, it might be necessary to define support points
522 to enhance and facilitate the interpolation to obtain a smoothed grid accounting also for
523 breakpoints. In case rates are not linear, and vary over time, the process will need to be
524 repeated for every period. For more details on the workflow, see Rijdsijk et al. (2025) who
525 present a correction grid for the Aegean Archipelago. In the future, we aim to facilitate this
526 procedure by creating (1) a point and linear feature database with topographic rates of
527 change, (2) an interpolation function, accounting for breakpoint features.

528

529 **Isolation metrics and visualisations:** We aim to further integrate more functionalities to
530 TABS, including other pre-calculated metrics than area change, such as distance between
531 shapes and timing of isolation. We also aim to integrate functions for default publication

532 ready visualisations including maps, connectivity metrics and curve changes for the selected
533 region or reconstructed shapes.

534 We encourage researchers interested in using TABS to contact our team for potential
535 collaborations, allowing us to better address user-specific needs and further optimize the tool
536 for diverse applications. For reporting bugs and recommendations, we advise to create an
537 issue in the TABS gitlab repository (https://gitlab.com/uva_ibed_piac/tabs/-/issues).

538

539 Conclusion

540 In conclusion, TABS is just as intuitive as pressing the *Tab* key—streamlining the complex
541 process of reconstructing spatio-temporal biogeographic configurations. By effortlessly
542 mapping surface area changes, connectivity, and isolation over time, TABS generates
543 structured geospatial datasets ready-to-use for further analysis and visualization. Its
544 customizable parameters can be adapted to any local environment, making it a valuable tool
545 for researchers aiming to model and quantify habitat changes over temporal scales, anywhere
546 on the globe.

547

548 **References**

- 549 Ali JR, Aitchison JC (2014) Exploring the combined role of eustasy and oceanic island thermal
550 subsidence in shaping biodiversity on the Galápagos. *Journal of Biogeography* 41:
551 1227–1241. <https://doi.org/10.1111/jbi.12313>
- 552 Bintanja R, van de Wal RSW (2008) North American ice-sheet dynamics and the onset of
553 100,000-year glacial cycles. *Nature* 454: 869–872.
554 <https://doi.org/10.1038/nature07158>
- 555 Bird P (2003) An updated digital model of plate boundaries. *Geochemistry, Geophysics,*
556 *Geosystems* 4. <https://doi.org/10.1029/2001GC000252>
- 557 Comes HP, Kadereit JW (1998) The effect of Quaternary climatic changes on plant
558 distribution and evolution. *Trends in Plant Science* 3: 432–438.
559 [https://doi.org/10.1016/S1360-1385\(98\)01327-2](https://doi.org/10.1016/S1360-1385(98)01327-2)
- 560 Cutler KB, Edwards RL, Taylor FW, Cheng H, Adkins J, Gallup CD, Cutler PM, Burr GS, Bloom
561 AL (2003) Rapid sea-level fall and deep-ocean temperature change since the last
562 interglacial period. *Earth and Planetary Science Letters* 206: 253–271.
563 [https://doi.org/10.1016/S0012-821X\(02\)01107-X](https://doi.org/10.1016/S0012-821X(02)01107-X)
- 564 De Groeve J, Norder S, Rijdsdijk KF (2024) Tiled version of GEBCO sub ice topo.
565 <https://doi.org/10.21942/uva.23943957.v3>
- 566 De Groeve J, Kusumoto B, Koene E, Kissling WD, Seijmonsbergen AC, Hoeksema BW,
567 Yasuhara M, Norder SJ, Cahyarini SY, van der Geer A, Meijer HJM, Kubota Y, Rijdsdijk
568 KF (2022a) Global raster dataset on historical coastline positions and shelf sea
569 extents since the Last Glacial Maximum. *Global Ecology and Biogeography* 31: 2162–
570 2171. <https://doi.org/10.1111/geb.13573>
- 571 De Groeve J, Kusumoto B, Koene E, Kissling WD, Seijmonsbergen AC, Hoeksema BW,
572 Yasuhara M, Norder SJ, Cahyarini SY, Geer A van der, Meijer HJM, Kubota Y, Rijdsdijk
573 KF (2022b) Spatio-Temporal Relative Sea Level Curve (RSL).
574 <https://doi.org/10.21942/uva.20029991.v1>
- 575 De Groeve JD, Norder SJ, Rijdsdijk KF, Flantua S, rentier eline (2023) Island, archipelago,
576 plate, mountain and point labeling dataset.
577 <https://doi.org/10.21942/uva.22788464.v5>
- 578 Dirnböck T, Essl F, Rabitsch W (2011) Disproportional risk for habitat loss of high-altitude
579 endemic species under climate change. *Global Change Biology* 17: 990–996.
580 <https://doi.org/10.1111/j.1365-2486.2010.02266.x>
- 581 Fernández-Palacios JM, Rijdsdijk KF, Norder SJ, Otto R, de Nascimento L, Fernández-Lugo S,
582 Tjørve E, Whittaker RJ (2016) Towards a glacial-sensitive model of island
583 biogeography. *Global Ecology and Biogeography* 25: 817–830.
584 <https://doi.org/10.1111/geb.12320>

- 585 Flantua S, Hooghiemstra H (2018) Historical connectivity and mountain biodiversity.
586 Available from: [https://www.semanticscholar.org/paper/Historical-connectivity-and-](https://www.semanticscholar.org/paper/Historical-connectivity-and-mountain-biodiversity-Flantua-Hooghiemstra/c7a44200cca79297ca5a0b6ed3c065132bc66615)
587 [mountain-biodiversity-Flantua-](https://www.semanticscholar.org/paper/Historical-connectivity-and-mountain-biodiversity-Flantua-Hooghiemstra/c7a44200cca79297ca5a0b6ed3c065132bc66615)
588 [Hooghiemstra/c7a44200cca79297ca5a0b6ed3c065132bc66615](https://www.semanticscholar.org/paper/Historical-connectivity-and-mountain-biodiversity-Flantua-Hooghiemstra/c7a44200cca79297ca5a0b6ed3c065132bc66615) (December 23,
589 2024).
- 590 Flantua SG, Hooghiemstra H, Van Boxel JH, Cabrera M, González-Carranza Z, González-
591 Arango C (2014) Connectivity dynamics since the Last Glacial Maximum in the
592 northern Andes; a pollen-driven framework to assess potential migration.
593 *Paleobotany and Biogeography: A Festschrift for Alan Graham in His 80th Year.*
594 Missouri Botanical Garden, St. Louis: 98–123. Available from:
595 [https://www.academia.edu/download/41747781/Connectivity_dynamics_since_the](https://www.academia.edu/download/41747781/Connectivity_dynamics_since_the_Last_Gla20160129-16042-t953fg.pdf)
596 [_Last_Gla20160129-16042-t953fg.pdf](https://www.academia.edu/download/41747781/Connectivity_dynamics_since_the_Last_Gla20160129-16042-t953fg.pdf) (February 25, 2025).
- 597 Flantua SGA, O’Dea A, Onstein RE, Giraldo C, Hooghiemstra H (2019) The flickering
598 connectivity system of the north Andean páramos. *Journal of Biogeography* 46:
599 1808–1825. <https://doi.org/10.1111/jbi.13607>
- 600 Flantua SGA, Payne D, Borregaard MK, Beierkuhnlein C, Steinbauer MJ, Dullinger S, Essl F, Irl
601 SDH, Kienle D, Kreft H, Lenzner B, Norder SJ, Rijsdijk KF, Rumpf SB, Weigelt P, Field R
602 (2020) Snapshot isolation and isolation history challenge the analogy between
603 mountains and islands used to understand endemism. *Global Ecology and*
604 *Biogeography* 29: 1651–1673. <https://doi.org/10.1111/geb.13155>
- 605 GEBCO Bathymetric Compilation G (2024) GEBCO_2024 Grid. British Oceanographic Data
606 Centre. <https://doi.org/10.5285/1c44ce99-0a0d-5f4f-e063-7086abc0ea0f>
- 607 GeoNames (2023) GeoNames. Available from:
608 <https://download.geonames.org/export/dump/> (February 25, 2025).
- 609 Hewitt G (2000) The genetic legacy of the Quaternary ice ages. *Nature* 405: 907–913.
610 <https://doi.org/10.1038/35016000>
- 611 Huang J-L, Andrello M, Martensen AC, Saura S, Liu D-F, He J-H, Fortin M-J (2020) Importance
612 of spatio-temporal connectivity to maintain species experiencing range shifts.
613 *Ecography* 43: 591–603. <https://doi.org/10.1111/ecog.04716>
- 614 Intergovernmental Panel on Climate Change (IPCC) (Ed.) (2023) Atlas. In: *Climate Change*
615 *2021 – The Physical Science Basis: Working Group I Contribution to the Sixth*
616 *Assessment Report of the Intergovernmental Panel on Climate Change.* Cambridge
617 University Press, Cambridge, 1927–2058.
618 <https://doi.org/10.1017/9781009157896.021>
- 619 Kealy S, Louys J, O’Connor S (2017) Reconstructing Palaeogeography and Inter-island
620 Visibility in the Wallacean Archipelago During the Likely Period of Sahul Colonization,
621 65–45 000 Years Ago. *Archaeological Prospection* 24: 259–272.
622 <https://doi.org/10.1002/arp.1570>

- 623 Kealy S, Louys J, O'Connor S (2018) Least-cost pathway models indicate northern human
624 dispersal from Sunda to Sahul. *Journal of Human Evolution* 125: 59–70.
625 <https://doi.org/10.1016/j.jhevol.2018.10.003>
- 626 Lambeck K, Rouby H, Purcell A, Sun Y, Sambridge M (2014) Sea level and global ice volumes
627 from the Last Glacial Maximum to the Holocene. *Proceedings of the National*
628 *Academy of Sciences* 111: 15296–15303. <https://doi.org/10.1073/pnas.1411762111>
- 629 Martensen AC, Saura S, Fortin M-J (2017) Spatio-temporal connectivity: assessing the
630 amount of reachable habitat in dynamic landscapes. *Methods in Ecology and*
631 *Evolution* 8: 1253–1264. <https://doi.org/10.1111/2041-210X.12799>
- 632 McGuire JL, Lawler JJ, McRae BH, Nuñez TA, Theobald DM (2016) Achieving climate
633 connectivity in a fragmented landscape. *Proceedings of the National Academy of*
634 *Sciences* 113: 7195–7200. <https://doi.org/10.1073/pnas.1602817113>
- 635 Norder SJ, Baumgartner JB, Borges PAV, Hengl T, Kissling WD, van Loon EE, Rijdsdijk KF (2018)
636 A global spatially explicit database of changes in island palaeo-area and archipelago
637 configuration during the late Quaternary. *Global Ecology and Biogeography* 27: 500–
638 505. <https://doi.org/10.1111/geb.12715>
- 639 Norder SJ, Proios K, Whittaker RJ, Alonso MR, Borges PAV, Borregaard MK, Cowie RH,
640 Florens FBV, de Frias Martins AM, Ibáñez M, Kissling WD, de Nascimento L, Otto R,
641 Parent CE, Rigal F, Warren BH, Fernández-Palacios JM, van Loon EE, Triantis KA,
642 Rijdsdijk KF (2019) Beyond the Last Glacial Maximum: Island endemism is best
643 explained by long-lasting archipelago configurations. *Global Ecology and*
644 *Biogeography* 28: 184–197. <https://doi.org/10.1111/geb.12835>
- 645 Papadopoulou A, Knowles LL (2015) Genomic tests of the species-pump hypothesis: Recent
646 island connectivity cycles drive population divergence but not speciation in
647 Caribbean crickets across the Virgin Islands. *Evolution* 69: 1501–1517.
648 <https://doi.org/10.1111/evo.12667>
- 649 Papadopoulou A, Knowles LL (2017) Linking micro- and macroevolutionary perspectives to
650 evaluate the role of Quaternary sea-level oscillations in island diversification.
651 *Evolution* 71: 2901–2917. <https://doi.org/10.1111/evo.13384>
- 652 Rangel TF, Edwards NR, Holden PB, Diniz-Filho JAF, Gosling WD, Coelho MTP, Cassemiro FAS,
653 Rahbek C, Colwell RK (2018) Modeling the ecology and evolution of biodiversity:
654 Biogeographical cradles, museums, and graves. *Science* 361: eaar5452.
655 <https://doi.org/10.1126/science.aar5452>
- 656 Rijdsdijk KF, Hengl T, Norder SJ, Otto R, Emerson BC, Ávila SP, López H, van Loon EE, Tjørve E,
657 Fernández-Palacios JM (2014a) Quantifying surface-area changes of volcanic islands
658 driven by Pleistocene sea-level cycles: biogeographical implications for the
659 Macaronesian archipelagos. *Journal of Biogeography* 41: 1242–1254.
660 <https://doi.org/10.1111/jbi.12336>

- 661 Rijdsdijk KF, Hengl T, Norder SJ, Otto R, Emerson BC, Ávila SP, López H, van Loon EE, Tjørve E,
662 Fernández-Palacios JM (2014b) Quantifying surface-area changes of volcanic islands
663 driven by Pleistocene sea-level cycles: biogeographical implications for the
664 Macaronesian archipelagos. *Journal of Biogeography* 41: 1242–1254.
665 <https://doi.org/10.1111/jbi.12336>
- 666 Rull V, Nogué S (2007) Potential migration routes and barriers for vascular plants of the
667 Neotropical Guyana Highlands during the Quaternary. *Journal of Biogeography* 34:
668 1327–1341. <https://doi.org/10.1111/j.1365-2699.2006.01602.x>
- 669 Sandel B, Arge L, Dalsgaard B, Davies RG, Gaston KJ, Sutherland WJ, Svenning J-C (2011) The
670 Influence of Late Quaternary Climate-Change Velocity on Species Endemism. *Science*
671 334: 660–664. <https://doi.org/10.1126/science.1210173>
- 672 Sayre R, Noble S, Hamann S, Smith R, Wright D, Breyer S, Butler K, Van Graafeiland K, Frye C,
673 Karagulle D, Hopkins D, Stephens D, Kelly K, Basher Z, Burton D, Cress J, Atkins K, Van
674 Sistine DP, Friesen B, Allee R, Allen T, Aniello P, Asaad I, Costello MJ, Goodin K, Harris
675 P, Kavanaugh M, Lillis H, Manca E, Muller-Karger F, Nyberg B, Parsons R, Saarinen J,
676 Steiner J, Reed A (2019) A new 30 meter resolution global shoreline vector and
677 associated global islands database for the development of standardized ecological
678 coastal units. *Journal of Operational Oceanography* 12: S47–S56.
679 <https://doi.org/10.1080/1755876X.2018.1529714>
- 680 Simaiakis SM, Rijdsdijk KF, Koene EFM, Norder SJ, Van Boxel JH, Stocchi P, Hammoud C,
681 Kougioumoutzis K, Georgopoulou E, Van Loon E, Tjørve KMC, Tjørve E (2017)
682 Geographic changes in the Aegean Sea since the Last Glacial Maximum: Postulating
683 biogeographic effects of sea-level rise on islands. *Palaeogeography,*
684 *Palaeoclimatology, Palaeoecology* 471: 108–119.
685 <https://doi.org/10.1016/j.palaeo.2017.02.002>
- 686 Snethlage MA, Geschke J, Ranipeta A, Jetz W, Yoccoz NG, Körner C, Spehn EM, Fischer M,
687 Urbach D (2022) A hierarchical inventory of the world's mountains for global
688 comparative mountain science. *Scientific Data* 9: 149.
689 <https://doi.org/10.1038/s41597-022-01256-y>
- 690 Svenning J-C, Eiserhardt WL, Normand S, Ordonez A, Sandel B (2015) The Influence of
691 Paleoclimate on Present-Day Patterns in Biodiversity and Ecosystems. *Annual Review*
692 *of Ecology, Evolution, and Systematics* 46: 551–572.
693 <https://doi.org/10.1146/annurev-ecolsys-112414-054314>
- 694 Tan DJX, Gyllenhaal EF, Andersen MJ (2023) PleistoDist: A toolbox for visualising and
695 quantifying the effects of Pleistocene sea-level change on island archipelagos.
696 *Methods in Ecology and Evolution* 14: 496–504. <https://doi.org/10.1111/2041-210X.14024>
- 698 Torres V, Vandenberghe J, Hooghiemstra H (2005) An environmental reconstruction of the
699 sediment infill of the Bogotá basin (Colombia) during the last 3 million years from
700 abiotic and biotic proxies. *Palaeogeography, Palaeoclimatology, Palaeoecology* 226:
701 127–148. <https://doi.org/10.1016/j.palaeo.2005.05.005>

- 702 Valente LM, Phillimore AB, Etienne RS (2015) Equilibrium and non-equilibrium dynamics
703 simultaneously operate in the Galápagos islands. *Ecology Letters* 18: 844–852.
704 <https://doi.org/10.1111/ele.12461>
- 705 Weigelt P, Jetz W, Kreft H (2013a) Bioclimatic and physical characterization of the world's
706 islands. *Proceedings of the National Academy of Sciences* 110: 15307–15312.
707 <https://doi.org/10.1073/pnas.1306309110>
- 708 Weigelt P, Jetz W, Kreft H (2013b) Data from: Bioclimatic and physical characterization of
709 the world's islands. : 7051753 bytes. <https://doi.org/10.5061/DRYAD.FV94V>
- 710 Weigelt P, Steinbauer MJ, Cabral JS, Kreft H (2016) Late Quaternary climate change shapes
711 island biodiversity. *Nature* 532: 99–102. <https://doi.org/10.1038/nature17443>
- 712 Wetzel FT, Kissling WD, Beissmann H, Penn DJ (2012) Future climate change driven sea-level
713 rise: secondary consequences from human displacement for island biodiversity.
714 *Global Change Biology* 18: 2707–2719. [https://doi.org/10.1111/j.1365-](https://doi.org/10.1111/j.1365-2486.2012.02736.x)
715 [2486.2012.02736.x](https://doi.org/10.1111/j.1365-2486.2012.02736.x)
- 716 Whittaker RJ, Fernández-Palacios JM, Matthews TJ, Borregaard MK, Triantis KA (2017) Island
717 biogeography: Taking the long view of nature's laboratories. *Science* 357: eaam8326.
718 <https://doi.org/10.1126/science.aam8326>
- 719 Williams JW, Jackson ST, Kutzbach JE (2007) Projected distributions of novel and
720 disappearing climates by 2100 AD. *Proceedings of the National Academy of Sciences*
721 104: 5738–5742. <https://doi.org/10.1073/pnas.0606292104>

722

723 Acknowledgements

724 ESR and SGAF acknowledge financial support from Trond Mohn Stiftelse (TMS) and the
725 University of Bergen for the startup grant 'TMS2022STG03' to S.G.A.Flantua. JDG was
726 supported by institutional resources from the Computational Support Team of the Institute
727 for Biodiversity and Ecosystem Dynamics (IBED), University of Amsterdam (Netherlands).
728 We would like to thank scientific illustrator Miranta Kouvari for preparing the graphical
729 abstract and R logo supported by the grant 'TMS2022STG03' to S.G.A.Flantua and by IBED
730 institutional budgets.

731

732 [Author contributions statement](#)

733 JDG: Writing - Original draft, Writing - Review and Editing, Visualisation, Software, Data

734 curation, Methodology, Project Administration, Conceptualisation

735 SJN: Writing - Original draft, Writing - Review and Editing, Resources, Methodology, Project

736 Administration, Conceptualisation

737 KFR: Writing - Review and Editing, Project Administration, Methodology, Resources,

738 Conceptualisation

739 ESR: Writing - Review and Editing, Project Administration, Validation, Conceptualisation

740 SGAF: Writing - Review and Editing, Project Administration, Resources, Funding Acquisition,

741 Conceptualisation

742

743 [Data Accessibility Statement](#)

744 TABS is accessible via https://gitlab.com/uva_ibed_piac/tabs and upon acceptance will be

745 linked to Zenodo with the corresponding DOI and reference. We intend to also submit the

746 package to CRAN. All default global datasets can be accessed at Figshare (De Groeve et al.

747 2022b, 2023, 2024).

748